SUPPORTING INFORMATION

Native separation and metallation analysis of SOD1 protein from the human central nervous system: a methodological workflow

Stéphane Roudeau[1]*, Benjamin G. Trist[2], Asuncion Carmona[1], Katherine M. Davies[3], Glenda M. Halliday[3], Yann Rufin[4], Stéphane Claverol[5], Stijn J.M. Van Malderen[6,#], Gerald Falkenberg[6], Kay L. Double[2], Richard Ortega[1]*

[1]Univ. Bordeaux, CNRS, CENBG, UMR-5797, 19 Chemin du Solarium, F-33170 Gradignan, France

[2]Brain and Mind Centre and School of Medical Sciences (Neuroscience), Faculty of Medicine and Health, The University of Sydney, Camperdown, Sydney, New South Wales 2050 Australia

[3]Brain and Mind Centre and Faculty of Medicine and Health, School of Medical Sciences, The University of Sydney, Australia

[4]Plateforme Biochimie et Biophysique (BioProt), Univ. Bordeaux, France

[5]Plateforme Proteome, Univ. Bordeaux, France

[6]DESY Synchrotron, Hamburg, Germany

[#]Present address: Department of Chemistry, Ghent University, Campus De Sterre, Belgium

*Corresponding authors

Table of Contents

Supporting Information S1. Detailed experimental protocols and methods

Samples and sample preparation

Ethics approval was obtained from the University of Sydney Human Research Ethics Committee (approval number 2015/202 and 2019/309). These tissues are derived from six anatomical regions: anterior cingulate cortex (ACC), substantia nigra (SN), occipital cortex (Ocx), locus coeruleus (LC), dorsal spinal cord (dSpC) and ventral spinal cord (vSpC). Demographic and clinical information for these tissues are presented in Supporting Table S2. Fresh frozen brain tissues (120-319 mg) from the anterior cingulate cortex (ACC), substantia nigra (SN) and occipital cortex (OCx) of 8 individuals (cases 1 to 8, Supporting Tables S2 and S3) were used to perform IEF and metal analysis experiments without SEC. Soluble protein extracts were prepared under non-denaturating conditions as previously detailed[1,2]. Final soluble protein concentrations were approximately 2.5 mg/mL (2.2-2.9 mg/mL), measured using a bicinchoninic acid (BCA) assay according to manufacturer's instructions (Thermo Fisher Scientific). Additional samples of fresh frozen brain tissues from the LC, SN and OCx of 6 individuals (18-51 mg; cases 9 to 14, Supporting Tables S2 and S3), as well as fresh frozen tissues from the vSpC of 6 individuals (40-79 mg; cases 9 to 11 and 15 to 17, Supporting Tables S2 and S3) and dSpC of 3 individuals (52-60 mg; cases 15 to 17, Supporting Tables S2 and S3), were used to perform IEF and metal analysis experiments coupled with SEC on soluble protein extracts. For this second set of experiments, tissue homogenization was performed at 4°C with an electric homogenizer (Sigma Aldrich) in five volumes of 20 mM Tris-base pH 7.4 (Bio-Rad 161-0719) with protease inhibitors (1 µL/20 mg of tissue weight, Sigma Aldrich P8340). Sample homogenates were treated with DNAse I and RNase A, centrifuged at 30,000 g for 30 min at 4°C, and supernatant (1.0-4.0 mg protein/mL) collected and stored at -80°C until further analysis[1]. All solutions were prepared with ultrapure water (Fisher Chemical) and high-purity chemicals to avoid metal contaminants. Obvious blood vessels were

removed because of possible Cu and Zn contamination from erythrocytic SOD1 and tissues were rinsed prior to homogenization. A proportion of the α- and β-chains of Hb identified in SEC-IEF-processed extracts may also have originated from dopaminergic neurons, astrocytes and oligodendrocytes known to express these proteins in cortical tissues[3]. Assessment of the color of human tissue extracts constitutes a basic yet informative quality control step in this regard, with red-colored tissues being associated with higher risk of blood contamination.

Size exclusion chromatography (SEC)

Superdex 75 Increase resin (10/300 GL column, bed dimension 10 x 300 mm, composite of cross-linked agarose and dextran, GE Healthcare) is optimized for the separation of molecules between 3,000-70,000 Da (SOD1 - 32,000 Da). Absorbance was measured at 280 nm and 265 nm, corresponding to wavelengths of maximum absorbance for SOD1. Sample volume was adjusted to 250 µL with 100 mM ammonium acetate solution (pH 7.4), prior to injection in the 500 µL injection loop. Solutions were prepared with ultrapure water (Fisher Chemical), high-purity chemicals and were filtered through Stericup filters before use. This ammonium acetate solution was then used as an eluent with a flow rate of 500 µL/min, and eluate was collected in 500 µL fractions in plastic tubes, which were stored at -20°C until further utilization. Where indicated, centrifugal filters with 10 kDa molecular weight cutoff (Amicon Ultra-2 10K centrifugal filter devices) were used to concentrate the eluate fraction f11. Centrifugal concentration filters were tested but not retained in our final protocol for SOD1 native metallation analysis (see Supporting Information S9).

Native isoelectric focusing (native IEF)

Native IEF and metallation analysis experiments performed without SEC employed 17 cm IPG strips (pH 4.7–5.9; ReadyStrip™ IPG Strip, Bio-Rad) as previously described[1,4]. Briefly, IPG strips were rehydrated with

300 µL of brain protein extract (660-870 µg total protein), and focusing performed at 10°C using a Protean IEF Cell (Bio-Rad) with the following method: 250 V, 15 min, rapid ramp; 10000 V, 2 h, slow ramp; 10000 V, 40000 V.H, rapid ramp; maximum current 50 µA/strip. These strips were discontinued shortly thereafter by the manufacturer, prompting us to adopt narrower pH range Zoom® IPG strips (pH 4.5-5.5, 7 cm, Invitrogen) for subsequent IEF experiments. For native IEF experiments coupled with SEC, the total volume of SOD1-containing SEC fraction (f11, 500 µL, ~10 µg total protein) was used for rehydration of the Zoom® IPG strips. Because the maximum volume for a single rehydration is 140 µL with these strips, successive rehydration/desiccation/rehydration cycles were performed at 10°C until loading the total volume of SEC fraction f11, 500 µL. Focusing was then performed at 10°C in Protean IEF Cell System (Bio-Rad) using a step voltage sequence (200 V, 20 min, slow ramp; 450 V, 15 min, rapid ramp; 750 V, 15 min, rapid ramp; 2000 V, rapid ramp until 10,000 VH reached) with a maximum current of 50 µA/strip. The focusing was considered complete when residual intensity was lower than 4 µA/strip. Blank samples consisting in unused ReadyStrip™ IPG strips (Bio-Rad) and Zoom® IPG strips (Invitrogen) were both checked by PIXE and SXRF analyses. Cu and Zn were not detectable by PIXE (<LOD, Supporting Figure S10b). They were just above the LOD by SXRF but below the limit of quantification (LOQ) and did not contribute significantly to the Cu and Zn X-ray emission signal from samples (Supporting Figure S10d). cSOD1 was used as positive control with native IEF performed on IPG strips loaded with 10 µg of cSOD1 solution in 20 mM Tris-base pH 7.4. Before metal analysis, all samples were air dried within a laminar flow hood to prevent from airborne metallic contaminants.

SXRF analysis

The X-ray beam was not focused but collimated by crossed slits to a size of 0.5 x 1 mm^2 (horizontal x vertical) in order to excite the complete SOD1 area within the IPG gel homogeneously. Samples were scanned over ranges of 1 to 4 mm in 5 or 10 steps horizontally across the beam (10 to 30 s for each step)

at a photon flux of 1 x 10^{12} ph/s, while the X-ray fluorescence emission was detected by a silicon drift detector (Vortex EM, Hitachi High-Tech), calibrated on an Xspress3 Mini 125. Spectral peak deconvolution and integration of the Cu and Zn Kα and Kβ peaks was performed using the core of PyMca 5.5.0[5], which is based around a least-square optimization of a compound pseudo-Voigt fit model. Normalization to the incoming X-ray flux was applied via the photon flux measurement via Canberra PD300-500CB PIPS detectors behind the slits. Scatter, sum and escape peaks were taken into account. PyMca's STRIP background model correction was performed. The X-ray yields of Cu and Zn were calculated via in-house code using reference materials with a known Cu and Zn concentration in the range of 2-12 ng/cm². For this purpose, a solution of human erythrocyte SOD1 (Sigma Aldrich S9636) was also used as a reference after a quantitative measurement of Zn and Cu performed by PIXE using Micromatter™ XRF calibration standards. The calibration of integrated, background corrected peaks produces Cu and Zn concentrations for these samples, from which Cu/Zn atomic ratios could be calculated, which are reported in this work.

PIXE analysis

The analyses were carried out with a proton beam (3 MeV energy, 500-800 pA current and focused in a 5 µm spot) scanning the sample on a 600x600 µm² surface following a protocol initially developed for SOD1 metal analysis on yeast protein extracts[4]. The X-ray fluorescence emission was monitored by two lithium drifted silicon detectors (Sirius) located at 45° and 135° from the proton beam direction. The PIXE raw data were processed using Gupixwin 2.2.4[6]. In order to obtain quantitative results, Micromatter™ XRF calibration standards were used for the calibration of the X-ray detectors as previously described[7]. Cu/Zn atomic ratios were calculated from Cu and Zn areal mass (µg.cm^{-2}) obtained by PIXE and corrected with the atomic weight of the element.

Proteomic mass spectrometry

Sample preparation and protein digestion. SOD1 lane was cut out from NBT stained IPG strips. Gel pieces were destained in 25 mM ammonium bicarbonate 50% acetonitrile (ACN), rinsed twice in ultrapure water and shrunk in ACN for 10 min. After ACN removal, gel pieces were dried at room temperature, covered with trypsin solution (10 ng/µl in 50 mM NH_4HCO_3), rehydrated at 4°C for 10 min, and finally incubated overnight at 37°C. Gel pieces were then covered with 50 mM NH_4HCO_3 at room temperature for 15 min with rotary shaking. The supernatant was collected, and an H_2O/ACN/HCOOH (47.5:47.5:5) extraction solution was added onto gel slices for 15 min. Peptide extraction was repeated twice. All supernatants were pooled and dried in a vacuum centrifuge. Pellets were resuspended in 30 µL of water acidified with 0.1% formic acid and stored at -20°C.

Nanoscale liquid chromatography coupled to tandem mass spectrometry (nLC-MS/MS) analysis and label-free quantitative data analysis. Peptide digests were analyzed on an Ultimate 3000 nanoLC system (Dionex, Amsterdam, The Netherlands) coupled to a Electrospray Orbitrap Fusion™ Lumos™ Tribrid™ Mass Spectrometer (Thermo Fisher Scientific). Ten microliters of peptide digests were loaded onto a 300-µm-inner diameter x 5-mm C18 PepMapTM trap column (LC Packings) at a flow rate of 10 µL/min. Peptides were eluted from the trap column onto an analytical 75-mm id x 50-cm C18 Pep-Map column (LC Packings) with a 4–40% linear gradient of solvent B in 45 min (solvent A, 0.1% formic acid; solvent B, 0.1% formic acid in 80% ACN). The separation flow rate was set at 300 nL/min. The mass spectrometer operated in positive ion mode at a 1.8-kV needle voltage. Data were acquired using Xcalibur 4.3 software in a data-dependent mode. MS scans (m/z 375-1500) were recorded at a resolution of R = 120 000 (@ m/z 200) and an automatic gain control target of 4.10^5 ions collected within 50 ms. Dynamic exclusion was set to 60 s and top speed fragmentation in higher-energy collisional dissociation (HCD) mode was performed over a 3 s cycle. MS/MS scans with a target value of 2.10^3 ions were collected in the ion trap with a maximum fill time of 35 ms. Additionally, only +2 to +7 charged ions were selected for fragmentation. Others settings were as follows: no sheath nor auxiliary gas flow, heated capillary temperature, 275 °C; normalized HCD

collision energy of 30% and an isolation width of 1.6 m/z. Monoisotopic precursor selection (MIPS) was set to Peptide and an intensity threshold was set to 5.10^3.

Database search and results processing. Data were searched by SEQUEST through Proteome Discoverer 2.4 (Thermo Fisher Scientific) against Homo sapiens Reference Proteome Set database (Uniprot 2019-09; 74,218 entries). Spectra from peptides higher than 5000 Da or lower than 350 Da were rejected. The search parameters were as follows: mass accuracy of the MIPS precursor and peptide fragments was set to 10 ppm and 0.6 Da respectively. Only b- and y-ions were considered for mass calculation. Oxidation of methionines (+16 Da) and protein N-terminal modifications (Acetylation +42Da; Methionine loss -131Da, Methionine-loss+Acetylation -89Da) were considered as variable modifications and carbamidomethylation of cysteines (+57 Da) as fixed modification. Two missed trypsin cleavages were allowed. Peptide validation was performed using Percolator algorithm[8] and only "high confidence" peptides were retained corresponding to a 1% False Positive Rate at peptide level. Protein abundancies are calculated as the sum of the abundancies of unique peptide intensities, measured in Mass Spectrometry by the Area Under the Curve by the Minora algorithm embedded in Proteome Discoverer.

Statistical analysis

Rstudio 1.2.5033[9], R software[10] v3.6.3 and associated packages tidyverse v1.3.0[11], Rcommander[12] v2.6-2, rstatix 0.4.0 (https://rpkgs.datanovia.com/rstatix/) and ggpubr 0.2.5 (https://rpkgs.datanovia.com/ggpubr/) were used for statistical analysis and plotting. The normality of dataset distributions was tested with the Shapiro test and the homogeneity of variances with the Bartlett's test. Comparisons between two groups were performed with Wilcoxon-Mann-Whitney test when the normality of the distributions was not met. Comparisons between three groups or more were performed with Kruskal-Wallis test when assumptions of normality of distributions or homogeneity of variances were not met. When Kruskal-Wallis test was considered significant (p-value <0.01), post-hoc multiple

comparisons were investigated with Dunn's test and p-values adjusted for pairwise comparisons (Holm's method). Details are presented in the associated content section (Supporting Table S13).

Supporting Table S2. Demographic information for post-mortem human tissue cases

Case number	Age (years)	Sex	Post-mortem delay (hours)	Cause of death	Anatomical regions studied
1	102	Female	5	Acute renal failure	ACC, SN, OCx
2	92	Female	5	Pancytopaenia	ACC, SN, OCx
3	103	Male	20	Acute myocardial infarct	ACC, SN, OCx
4	74	Male	16.5	Toxicity	ACC, SN, OCx
5	41	Male	48	Cardiorespiratory failure	ACC, SN, OCx
6	65	Male	14.5	Cardiorespiratory failure	ACC, SN, OCx
7	49	Male	47	Cardiorespiratory failure	ACC, SN
8	28	Male	28	Toxicity	ACC, SN, OCx
9	63	Male	23	Unknown	LC, vSpC
10	73	Female	27	Unknown	LC, vSpC
11	51	Female	33	Unknown	LC, vSpC
12	89	Male	33	Cardiorespiratory failure	SN, OCx
13	91	Male	13	Cardiorespiratory failure	SN, OCx
14	85	Female	23	Pneumonia	SN, OCX
15	48	Male	6.5	Cardiorespiratory failure	vSpC, dSpC
16	55	Male	5	Cardiorespiratory failure	vSpC, dSpC
17	49	Male	6.1	Cardiorespiratory failure	vSpC, dSpC

Table S2. Demographic information for post-mortem human tissue cases. ACC: anterior cingulate cortex; SN: substantia nigra; OCx: occipital cortex; LC: locus coeruleus; dSpC: dorsal spinal cord; vSpC: ventral spinal cord.

Supporting Table S3. Information for post-mortem human tissues

Case number	Anatomical region	Tissue mass (mg), frozen hydrated	Applied separation procedure
1	ACC	277.00	IEF
1	SN	260.00	IEF
1	OCx	280.00	IEF
2	ACC	248.00	IEF
2	SN	273.00	IEF
2	OCx	279.00	IEF
3	ACC	261.00	IEF
3	SN	275.00	IEF
3	OCx	269.00	IEF
4	ACC	282.00	IEF
4	SN	120.00	IEF
4	OCx	251.00	IEF
5	ACC	258.00	IEF
5	SN	210.00	IEF
5	OCx	319.00	IEF
6	ACC	244.00	IEF
6	SN	162.00	IEF
6	OCx	255.00	IEF
7	ACC	288.00	IEF
7	SN	154.00	IEF
8	ACC	245.00	IEF
8	SN	240.00	IEF
8	OCx	235.00	IEF
9	LC	38.00	IEF+SEC
9	vSpC	47.00	IEF+SEC
10	LC	18.00	IEF+SEC
10	vSpC	40.00	IEF+SEC
11	LC	24.00	IEF+SEC
11	vSpC	79.00	IEF+SEC
12	SN	41.00	IEF+SEC
12	OCx	40.00	IEF+SEC
13	SN	30.00	IEF+SEC
13	OCx	45.00	IEF+SEC
14	SN	30.00	IEF+SEC
14	OCx	51.00	IEF+SEC
15	vSpC	66.30	IEF+SEC
15	dSpC	52.20	IEF+SEC

16	dSpC	55.70	IEF+SEC
16	vSpC	40.40	IEF+SEC
17	vSpC	64.20	IEF+SEC
17	dSpC	60.40	IEF+SEC

Supporting Table S3. Information for post-mortem human tissues. ACC: anterior cingulate cortex; SN: substantia nigra; OCx: occipital cortex; LC: locus coeruleus; dSpC: dorsal spinal cord; vSpC: ventral spinal cord; IEF: native isoelectric focusing; SEC: size-exclusion chromatography.

Supporting Table S4. Proteomic mass spectrometry analysis of SOD1 gel band after native IEF only

Accession	Description	Abundance	Cu or Zn binding (accord. Uniprot)	Relative abundance	Relative abundance to SOD1	Rank
P19652	14-3-3 protein zeta/delta OS=Homo sapiens OX=9606 GN=YWHAZ PE=1 SV=1	15074956636		10.2%	1573.1%	1
P09936	Ubiquitin carboxyl-terminal hydrolase isozyme L1 OS=Homo sapiens OX=9606 GN=UCHL1 PE=1 SV=2	8734363708		5.9%	911.5%	2
P62258	14-3-3 protein epsilon OS=Homo sapiens OX=9606 GN=YWHAE PE=1 SV=1	8214659059		5.6%	857.2%	3
A0A1C7CYX9	Dihydropyrimidinase-related protein 2 OS=Homo sapiens OX=9606 GN=DPYSL2 PE=1 SV=1	7426913464		5.0%	775.0%	4
P02768	Serum albumin OS=Homo sapiens OX=9606 GN=ALB PE=1 SV=2	6095905639	Cu, Zn	4.1%	636.1%	5
P12277	Creatine kinase B-type OS=Homo sapiens OX=9606 GN=CKB PE=1 SV=1	5558375610		3.8%	580.0%	6
E9PLK3	Aminopeptidase OS=Homo sapiens OX=9606 GN=NPEPPS PE=1 SV=1	4509056234	Zn	3.0%	470.5%	7
P27348	14-3-3 protein theta OS=Homo sapiens OX=9606 GN=YWHAQ PE=1 SV=1	3886860482		2.6%	405.6%	8
P14618	Pyruvate kinase PKM OS=Homo sapiens OX=9606 GN=PKM PE=1 SV=4	3649749328		2.5%	380.9%	9
P07195	L-lactate dehydrogenase B chain OS=Homo sapiens OX=9606 GN=LDHB PE=1 SV=2	3464962421		2.4%	361.6%	10
P18669	Phosphoglycerate mutase 1 OS=Homo sapiens OX=9606 GN=PGAM1 PE=1 SV=2	3076178014		2.1%	321.0%	11
P14136	Glial fibrillary acidic protein OS=Homo sapiens OX=9606 GN=GFAP PE=1 SV=1	2606776116		1.8%	272.0%	12

P02794	Ferritin heavy chain OS=Homo sapiens OX=9606 GN=FTH1 PE=1 SV=2	2598192982		1.8%	271.1%	13
P09972	Fructose-bisphosphate aldolase C OS=Homo sapiens OX=9606 GN=ALDOC PE=1 SV=2	2443740378		1.7%	255.0%	14
P04406	Glyceraldehyde-3-phosphate dehydrogenase OS=Homo sapiens OX=9606 GN=GAPDH PE=1 SV=3	2198751028		1.5%	229.4%	15
P69905	Hemoglobin subunit alpha OS=Homo sapiens OX=9606 GN=HBA1 PE=1 SV=2	2170391268		1.5%	226.5%	16
P22314	Ubiquitin-like modifier-activating enzyme 1 OS=Homo sapiens OX=9606 GN=UBA1 PE=1 SV=3	2066833853		1.4%	215.7%	17
P61981	14-3-3 protein gamma OS=Homo sapiens OX=9606 GN=YWHAG PE=1 SV=2	1957059296		1.3%	204.2%	18
Q15149	Plectin OS=Homo sapiens OX=9606 GN=PLEC PE=1 SV=3	1710408541		1.2%	178.5%	19
P31947	14-3-3 protein sigma OS=Homo sapiens OX=9606 GN=SFN PE=1 SV=1	1536542855		1.0%	160.3%	20
Q04917	14-3-3 protein eta OS=Homo sapiens OX=9606 GN=YWHAH PE=1 SV=4	1509037141		1.0%	157.5%	21
P00338	L-lactate dehydrogenase A chain OS=Homo sapiens OX=9606 GN=LDHA PE=1 SV=2	1507872141		1.0%	157.4%	22
P31946	14-3-3 protein beta/alpha OS=Homo sapiens OX=9606 GN=YWHAB PE=1 SV=3	1429507163		1.0%	149.2%	23
P04075	Fructose-bisphosphate aldolase A OS=Homo sapiens OX=9606 GN=ALDOA PE=1 SV=2	1258454343		0.9%	131.3%	24
P68871	Hemoglobin subunit beta OS=Homo sapiens OX=9606 GN=HBB PE=1 SV=2	1174423392		0.8%	122.6%	25
P07900	Heat shock protein HSP 90-alpha OS=Homo sapiens OX=9606 GN=HSP90AA1 PE=1 SV=5	1117192533		0.8%	121.6%	26
P00441	**Superoxide dismutase [Cu-Zn] OS=Homo sapiens OX=9606 GN=SOD1 PE=1 SV=2**	**958285878**	**Cu, Zn**	**0.7%**	**100%**	**27**
	Omitted: 1208 proteins			*<0.7%*	*<100.0%*	
P08294	*Extracellular superoxide dismutase [Cu-Zn], SOD3*	*Not detected*				

Supporting Table S4. Proteomic mass spectrometry analysis of SOD1 gel band after native IEF only. Protein extract was prepared from human cerebral cortex. Tables show the main proteins detected in IEF gels at SOD1 location, without SEC prior to native IEF. Proteins are classified according to their relative abundance (rounded to the nearest 0.1%), only the first 27 proteins are shown.

Supporting Table S5. Proteomic mass spectrometry analysis of SOD1 gel band after SEC and native IEF

Accession	Description	Abundance	Cu or Zn binding (accord. Uniprot)	Relative abundance	Relative abundance to SOD1	Rank
P00441	**Superoxide dismutase [Cu-Zn] OS=Homo sapiens OX=9606 GN=SOD1 PE=1 SV=2**	**1095637388**	**Cu, Zn**	**64.5%**	**100.0%**	**1**
P69905	Hemoglobin subunit alpha OS=Homo sapiens OX=9606 GN=HBA1 PE=1 SV=2	126259641		7.4%	11.5%	2
P68871	Hemoglobin subunit beta OS=Homo sapiens OX=9606 GN=HBB PE=1 SV=2	77453633		4.6%	7.1%	3
P02768	Serum albumin OS=Homo sapiens OX=9606 GN=ALB PE=1 SV=2	40448040	Cu, Zn	2.4%	3.7%	4
P30041	Peroxiredoxin-6 OS=Homo sapiens OX=9606 GN=PRDX6 PE=1 SV=3	35669284		2.1%	3.3%	5
P0DP25	Calmodulin-3 OS=Homo sapiens OX=9606 GN=CALM3 PE=1 SV=1	26691309		1.6%	2.4%	6
H3BRV9	Nuclear transport factor 2 (Fragment) OS=Homo sapiens OX=9606 GN=NUTF2 PE=1 SV=1	17040155		1.0%	1.6%	7
O94760	N(G),N(G)-dimethylarginine dimethylaminohydrolase 1 OS=Homo sapiens OX=9606 GN=DDAH1 PE=1 SV=3	15885871	Zn	0.9%	1.4%	8
K7ELW0	Protein/nucleic acid deglycase DJ-1 OS=Homo sapiens OX=9606 GN=PARK7 PE=1 SV=1	9654417	Cu	0.6%	0.9%	9
P00558	Phosphoglycerate kinase 1 OS=Homo sapiens OX=9606 GN=PGK1 PE=1 SV=3	9180238		0.5%	0.8%	10

Q9Y5Z4	Heme-binding protein 2 OS=Homo sapiens OX=9606 GN=HEBP2 PE=1 SV=1	8865035		0.5%	0.8%	11
Q04760	Lactoylglutathione lyase OS=Homo sapiens OX=9606 GN=GLO1 PE=1 SV=4	8342620	Zn	0.5%	0.8%	12
P14550	Aldo-keto reductase family 1 member A1 OS=Homo sapiens OX=9606 GN=AKR1A1 PE=1 SV=3	8313450		0.5%	0.8%	13
F6TLX2	Glyoxalase domain-containing protein 4 OS=Homo sapiens OX=9606 GN=GLOD4 PE=1 SV=1	8096364		0.5%	0.7%	14
Q16658	Fascin OS=Homo sapiens OX=9606 GN=FSCN1 PE=1 SV=3	6912703		0.4%	0.6%	15
P09936	Ubiquitin carboxyl-terminal hydrolase isozyme L1 OS=Homo sapiens OX=9606 GN=UCHL1 PE=1 SV=2	6806381		0.4%	0.6%	16
P31150	Rab GDP dissociation inhibitor alpha OS=Homo sapiens OX=9606 GN=GDI1 PE=1 SV=2	6402341		0.4%	0.6%	17
P16152	Carbonyl reductase [NADPH] 1 OS=Homo sapiens OX=9606 GN=CBR1 PE=1 SV=3	6371944		0.4%	0.6%	18
Q9NX46	ADP-ribose glycohydrolase ARH3 OS=Homo sapiens OX=9606 GN=ADPRHL2 PE=1 SV=1	5901730		0.3%	0.5%	19
P15121	Aldo-keto reductase family 1 member B1 OS=Homo sapiens OX=9606 GN=AKR1B1 PE=1 SV=3	5431349		0.3%	0.5%	20
Q96JD6	1,5-anhydro-D-fructose reductase OS=Homo sapiens OX=9606 GN=AKR1E2 PE=1 SV=2	5117483		0.3%	0.5%	21
P50135	Histamine N-methyltransferase OS=Homo sapiens OX=9606 GN=HNMT PE=1 SV=1	5017808		0.3%	0.5%	22
Q15121	Astrocytic phosphoprotein PEA-15 OS=Homo sapiens OX=9606 GN=PEA15 PE=1 SV=2	4431919		0.3%	0.4%	23
P62258	14-3-3 protein epsilon OS=Homo sapiens OX=9606 GN=YWHAE PE=1 SV=1	4385142		0.3%	0.4%	24

P09211	Glutathione S-transferase P OS=Homo sapiens OX=9606 GN=GSTP1 PE=1 SV=2	4163950.		0.2%	0.4%	25
O95336	6-phosphogluconolactonase OS=Homo sapiens OX=9606 GN=PGLS PE=1 SV=2	3778116		0.2%	0.3%	26
P60174	Triosephosphate isomerase OS=Homo sapiens OX=9606 GN=TPI1 PE=1 SV=3	3686381		0.2%	0.3%	27
	Omitted: 323 proteins			*<0.2%*	*<0.3%*	
P08294	*Extracellular superoxide dismutase [Cu-Zn], SOD3*	*Not detected*				

Supporting Table S5. Proteomic mass spectrometry analysis of SOD1 gel band after SEC and native IEF. Protein extract was prepared from human cerebral cortex. Table show the main proteins detected in IEF gels at SOD1 location, with SEC performed before native IEF. Proteins are classified according to their relative abundance (rounded to the nearest 0.1%), only the first 27 proteins are shown

Supporting Table S6. Proteomic mass spectrometry analysis of cSOD1 gel band after SEC and native IEF

Accession	Description	Abundance	Cu or Zn binding (accord. Uniprot)	Relative abundance	Relative abundance to SOD1	Rank
P00441	**Superoxide dismutase [Cu-Zn] OS=Homo sapiens OX=9606 GN=SOD1 PE=1 SV=2**	**416729127**	**Cu, Zn**	**97.6%**	**100.00%**	**1**
P17174	Aspartate aminotransferase, cytoplasmic OS=Homo sapiens OX=9606 GN=GOT1 PE=1 SV=3	2892143		0.7%	0.7%	2
P04264	Keratin, type II cytoskeletal 1 OS=Homo sapiens OX=9606 GN=KRT1 PE=1 SV=6	2165553		0.5%	0.5%	3
P35908	Keratin, type II cytoskeletal 2 epidermal OS=Homo sapiens OX=9606 GN=KRT2 PE=1 SV=2	1399954		0.3%	0.3%	4
P13645	Keratin, type I cytoskeletal 10 OS=Homo sapiens OX=9606 GN=KRT10 PE=1 SV=6	1295591		0.3%	0.3%	5
P02768	Serum albumin OS=Homo sapiens OX=9606 GN=ALB PE=1 SV=2	631738	Cu, Zn	0.1%	0.2%	6
P35527	Keratin, type I cytoskeletal 9 OS=Homo sapiens OX=9606 GN=KRT9 PE=1 SV=3	539164		0.1%	0.1%	7
P02787	Serotransferrin OS=Homo sapiens OX=9606 GN=TF PE=1 SV=3	302429		0.1%	0.1%	8
A0A2R8Y7R2	Hemoglobin subunit beta OS=Homo sapiens OX=9606 GN=HBB PE=1 SV=1	136809		<0.1%	<0.1%	10
P63104	14-3-3 protein zeta/delta OS=Homo sapiens OX=9606 GN=YWHAZ PE=1 SV=1	126492		<0.1%	<0.1%	11
P19652	Alpha-1-acid glycoprotein 2 OS=Homo sapiens OX=9606 GN=ORM2 PE=1 SV=2	87217		<0.1%	<0.1%	12

P69905	Hemoglobin subunit alpha OS=Homo sapiens OX=9606 GN=HBA1 PE=1 SV=2	69825		<0.1%	<0.1%	13
K7EM20	14-3-3 protein epsilon (Fragment) OS=Homo sapiens OX=9606 GN=YWHAE PE=1 SV=1	48214		<0.1%	<0.1%	14
Q9Y4D1	Disheveled-associated activator of morphogenesis 1 OS=Homo sapiens OX=9606 GN=DAAM1 PE=1 SV=2	47625		<0.1%	<0.1%	15
H0YIN9	Keratin, type II cytoskeletal 5 (Fragment) OS=Homo sapiens OX=9606 GN=KRT5 PE=1 SV=1	46174		<0.1%	<0.1%	16
P60709	Actin, cytoplasmic 1 OS=Homo sapiens OX=9606 GN=ACTB PE=1 SV=1	41783		<0.1%	<0.1%	17
O75368	SH3 domain-binding glutamic acid-rich-like protein OS=Homo sapiens OX=9606 GN=SH3BGRL PE=1 SV=1	37382		<0.1%	<0.1%	18
Q16555	Dihydropyrimidinase-related protein 2 OS=Homo sapiens OX=9606 GN=DPYSL2 PE=1 SV=1	9716		<0.1%	<0.1%	19
P05787	Keratin, type II cytoskeletal 8 OS=Homo sapiens OX=9606 GN=KRT8 PE=1 SV=7	9404		<0.1%	<0.1%	20
H3BR70	Pyruvate kinase OS=Homo sapiens OX=9606 GN=PKM PE=1 SV=1	4625		<0.1%	<0.1%	21
	Omitted: none					
P08294	*Extracellular superoxide dismutase [Cu-Zn], SOD3*	*Not detected*				

Supporting Table S6. Proteomic mass spectrometry analysis of cSOD1 gel band. Commercial human superoxide dismutase (cSOD1) was used as a positive control and submitted to SEC + IEF before being analyzed by mass spectrometry. Proteins are classified according to their relative abundance (rounded to the nearest 0.1%).

Supporting Information S7. SOD1 protein conformation is preserved during SEC

The pI of a protein derives from the combined charges of all solvent-exposed amino acid residues within that protein, and therefore changes in pI represent alterations to gross protein conformation[13]. To verify that purification of SOD1 using SEC did not alter pI, and thus native conformation of the enzyme, we measured the pI of enzymatically-active SOD1 in focused IPG gels before and after SEC using NBT activity staining. Gels were loaded with either a commercially-available positive control solution of human SOD1 (cSOD1), or a soluble protein extract derived from 40 mg of human occipital cortex. The SEC absorption chromatogram of the cSOD1 solution exhibited one well-delineated peak at 11.81 ± 0.10 mL (mean ± SD, n=6 over 4 cycles of column use) (Supporting Figure S8a), reflecting elution of cSOD1 within SEC fraction 11 (f11). NBT staining intensity profiles of focused IPG gels were identical between SEC-processed and unprocessed cSOD1 solutions, with a main isoform at pI 5.06 and a minor one at 4.97 (red triangles; Supporting Figure S8c). Similarly, NBT staining revealed two active SOD1 isoforms at pI 5.00 and 5.09 in SEC-processed and unprocessed human occipital cortex extracts (Supporting Figure S8d). It is noteworthy that the SEC absorption chromatogram of the human occipital cortical extract did not exhibit one clear peak at f11 (Supporting Figure S8b), consistent with an increased proteomic complexity and relatively low abundance of SOD1 protein within these crude tissue extracts. The pI 5.00 active SOD1 isoform was determined to be the primary, most abundant isoform as it consistently gave a very clear signal and a wide achromatic band following NBT staining (Supporting Figure S8d). In contrast, the signal intensity of the pI 5.09 isoform was markedly lower and appeared as a diffuse achromatic band. These findings demonstrate that SOD1 protein conformation is preserved during SEC.

Supporting Figure S8. Effect of SEC on pI and enzymatic activity of SOD1

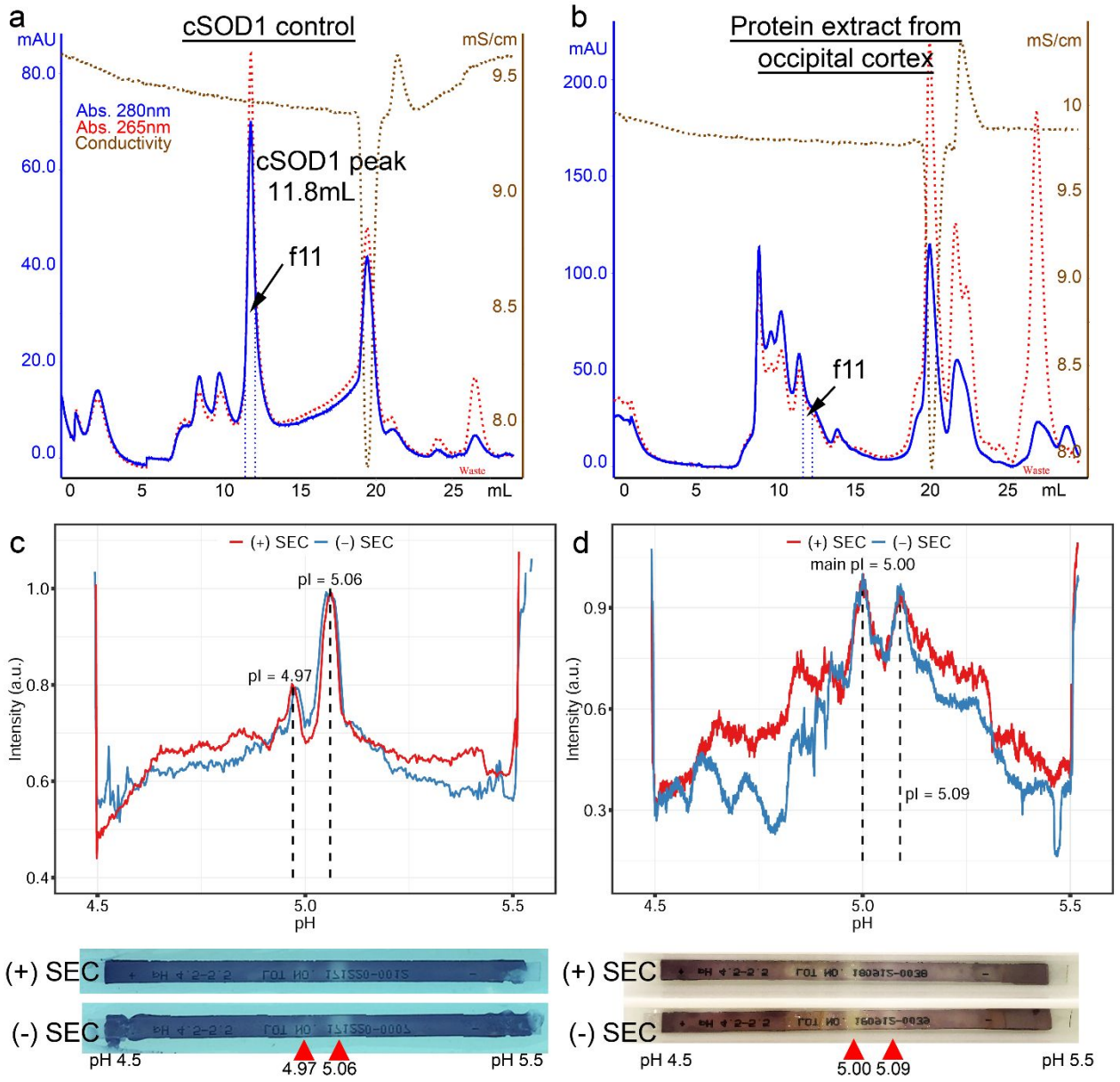

Supporting Figure S8. Effect of SEC on pI and enzymatic activity of SOD1. (a) SEC absorption chromatograms of cSOD1 used as a positive control. cSOD1 (126 µg) was injected into the SEC column and the elution peak identified within fraction 11 (f11, 11.8 mL). (b) SEC absorption chromatogram of brain

tissue protein extract prepared from 40 mg of human occipital cortex. Fraction 11, containing SOD1, was used for further analyses. (c) The pI of control cSOD1 (10 µg) was determined before SEC (-SEC, blue line) and after SEC (+SEC, red line, f11) by native IEF and NBT staining. Intensity quantification of the NBT staining shows a main isoform at pI 5.06 and a minor isoform at pI 4.97 and confirms that SEC procedure does not affect the pI of the control cSOD1. (d) The pI of SOD1 in protein extract from occipital cortex (-SEC, blue line) was compared to the pI of SOD1 after SEC (+SEC, red line) in the corresponding fraction f11, using native IEF and NBT staining. Intensity quantification of the NBT staining demonstrated a major (pI 5.00) and a minor (pI 5.09) isoform, the net charges of which were unaffected by SEC.

Supporting Information S9. Cu/Zn ratio of cSOD1 protein is unchanged following SEC and native IEF

As alterations to SOD1 pI are associated with SOD1 mismetallation[4], preservation of SOD1 pI during SEC and native IEF suggests our purification protocol does not alter SOD1 metallation. To confirm this, we measured the Cu/Zn ratio of cSOD1 at different stages of our purification protocol using PIXE and SXRF (Supporting Figure S10 and S11, Supporting Table S12). Measurements were made: (i) in an untreated cSOD1 solution deposited on an ultrapure polycarbonate (PC) foil, (ii) in focused IPG gels following native IEF and (iii) in IPG gels following native two-dimensional fractionation (SEC-IEF). No significant differences in the Cu/Zn ratio of cSOD1 were observed between each set of conditions, confirming that neither SEC nor native IEF alters SOD1 metal binding (Supporting Figure S11). Elemental analyses of blank IPG gels demonstrated that Cu and Zn levels were below the quantification limits (Supporting Figure S10, blank spectra in red), indicating that metal analyses were not confounded by Cu or Zn contamination from solutions or gels used for native IEF, or from the sample environment during X-ray analysis. For PIXE analyses, performed under secondary vacuum, only Cu and Zn were detected in the cSOD1 samples confirming the absence of metal contamination. For all SXRF analyses, blanks and cSOD1 samples, some additional elements (Cr 5.4 keV, Mn 5.9 keV, Fe 6.4 keV, and Co 6.9 keV) were detected but with very low counting rates (Supporting Figure S10c). These elements are associated with the scattering of the incident beam on stainless steel components from the analytical environment, because of the very high sensitivity of SXRF, and despite this contribution was reduced to the minimum during the experiments. Since SXRF analyses were performed in air, a large peak for argon was also present in spectra (3.0 keV), however these contributions did not disturb Cu (8.0 keV) or Zn (8.6 keV) quantification. In contrast to the protein separation using SEC and IEF, we identified significant alterations to cSOD1 metal content following the use of centrifugal concentration filters (10 kDa molecular weight cutoff), which were initially investigated

as a means to reduce the volume of f11 following SEC (500 µL) to the appropriate 140 µL rehydration volume for native IEF. Use of centrifugal concentration filters was associated with a significant increase in the ratio of Cu/Zn bound to cSOD1 (Supporting Figure S11, Supporting Table S12), prompting us to adopt a direct concentration approach to load the SOD1-containing SEC fractions for native IEF by multiple cycles of rehydration/desiccation/rehydration (see Supporting Information S1, Native isoelectric focusing (native IEF)). It is unclear whether this alteration of Cu/Zn ratio derives from cSOD1 Zn demetallation or Cu supplementation, but the overall effect is similar to that observed with silica-based columns associated with Cu re-metallation of apo-SOD1[14]. These data highlight the importance of step-by-step protocol validation throughout metallation studies to ensure maintenance of endogenous protein metal binding.

Supporting Figure S10. Cu/Zn ratio in cSOD1 separated by SEC and IEF

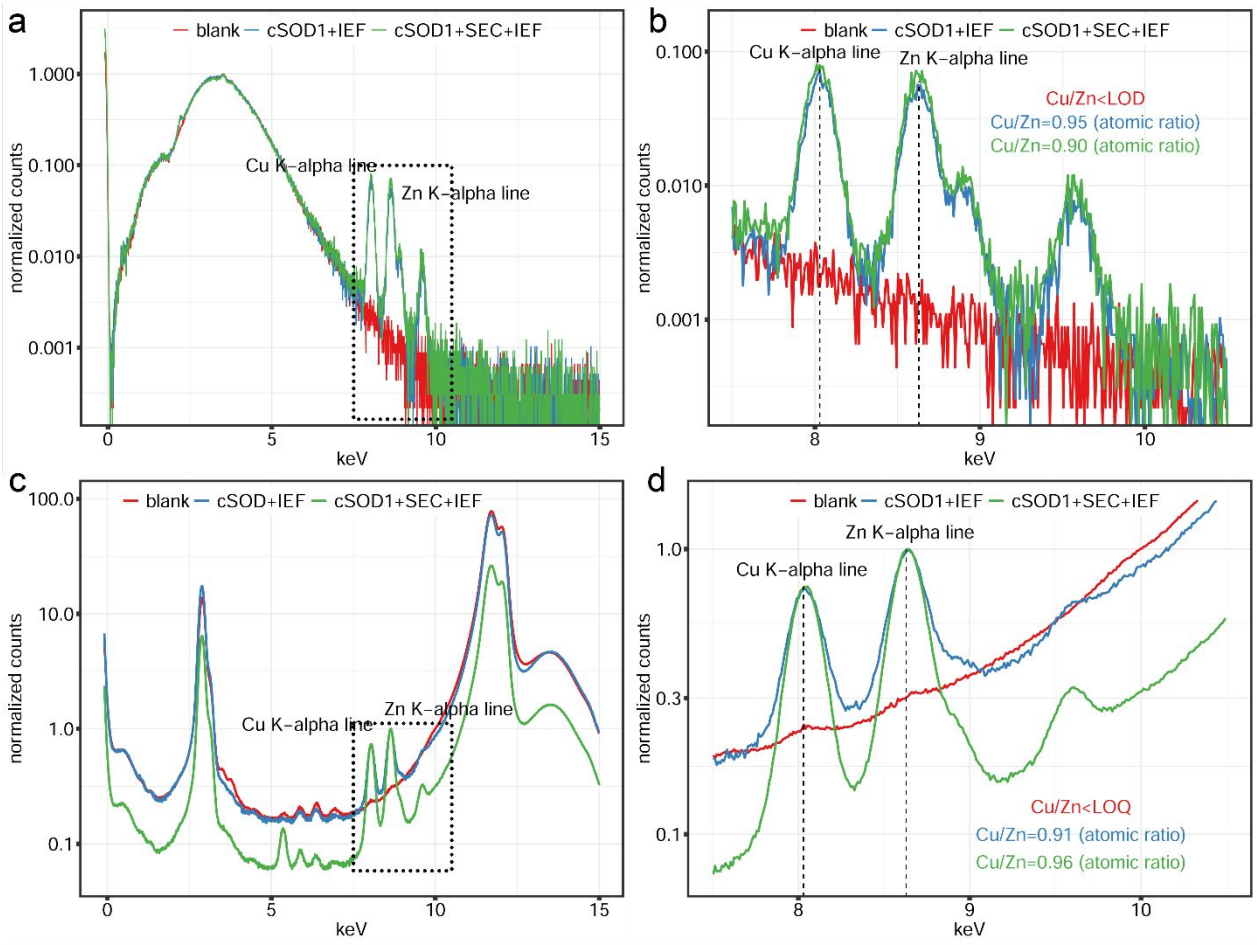

Supporting Figure S10. Cu/Zn ratio in cSOD1 separated by SEC and IEF. Control cSOD1 (10 µg) was separated by native IEF or by both SEC and native IEF prior to metal analyses by PIXE (a, b) and SXRF (c, d), blank IPG strips were used as controls (red line). Panels (a) and (c) show respectively two representative PIXE and SXRF spectra of cSOD1 measured after native IEF (cSOD1 + IEF, blue line), and SEC + native IEF (cSOD1 + SEC + IEF, green line). (b, d) Zoom on the Cu and Zn energy regions of spectra (a) and (c) with respective Cu/Zn atomic ratio values.

Supporting Figure S11. Boxplots median quartile and interquartile range for Cu/Zn atomic ratio of cSOD1 measured by PIXE and SXRF

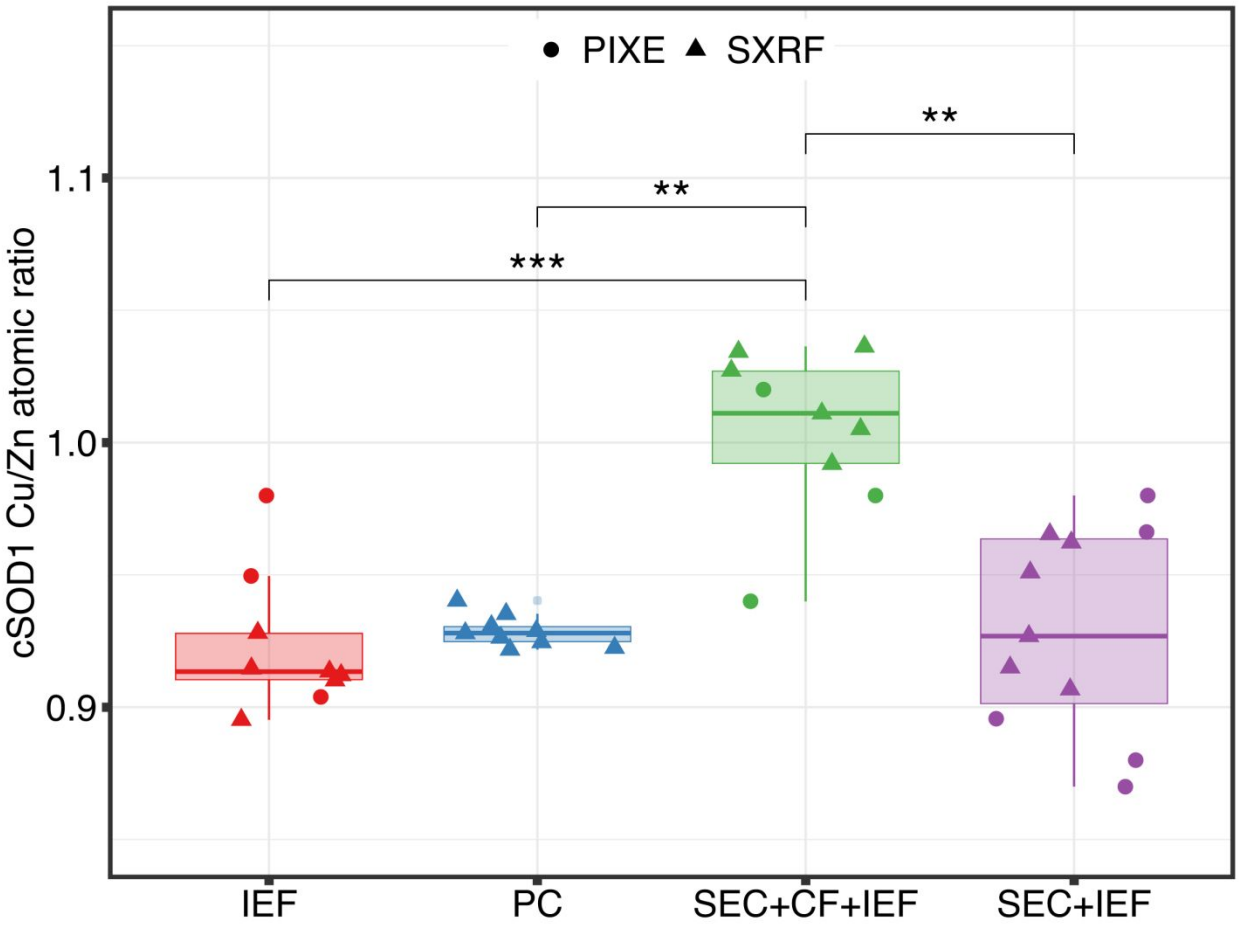

Supporting Figure S11. Boxplots median quartile and interquartile range for Cu/Zn atomic ratio of cSOD1 measured by PIXE and SXRF after (i) native IEF (IEF), (ii) direct deposition onto polycarbonate foils (PC), (iii) SEC + centrifugal concentration filter + native IEF (SEC+CF+IEF) and (iv) SEC + native IEF (SEC+IEF). Mean values and sd are presented in Supporting Table S12. Whilst neither SEC nor IEF alter the ratio of Cu/Zn bound to cSOD1, centrifugal concentration filters substantially increase this ratio (Kruskall Wallis test, Dunn's post-hoc multiple comparisons); **p<0.01, *** p< 0.001; Supporting Table S13 for details).

Supporting Table S12. Mean Cu/Zn ratio of commercial cSOD1 at different stages of our purification protocol

	Cu/Zn ratio		
Procedure	Mean	Standard deviation	n
PC	0.93	0.01	9
IEF	0.92	0.03	9
SEC + CF + IEF	1.01	0.03	9
SEC + IEF	0.93	0.04	11

Supporting Table S12. Mean Cu/Zn ratio of commercial cSOD1 at different stages of our purification protocol. Metal measurements were performed directly after deposition onto a polycarbonate foil (PC), or within the SOD1-containing gel band of focused IPG strips after native IEF (IEF), after SEC + concentration filter 10 kDa + native IEF (SEC+CF+IEF), and after SEC + native IEF (SEC+IEF). Corresponding data depicted within Supporting Figure S11.

Supporting Table S13. Statistical analysis of data

Figure	Data	Population size	Distribution normality (Shapiro-Wilk test) p<0.05 : data deviate from normal distribution	Variance homogeneity (Bartlett's test) p<0.05 : variances in each group are different	Statistical test
Figure 2c	Cu/Zn ratio of SOD1 from human brain tissues and spinal cord	Brain samples IEF n=23 Brain samples SEC+IEF, n=18	Brain samples IEF, p=0.376 Brain samples SEC+IEF, p=0.0003	n. a.	Wilcoxon-Mann-Whitney P= 0.0033
Figure 2d	Cu/Zn ratio of SOD1 from human brain tissues and spinal cord	-SEC brain regions: ACC n=8 OCx n=7 SN n=8			Kruskall-Wallis p=0.610
Figure 2d	Cu/Zn ratio of SOD1 from human brain tissues and spinal cord	+SEC brain regions: dSpC n=3 LC n=3 OCx n=3 SN n=3 vSpC n=6			Kruskall-Wallis p=0.098
Supporting Figure S9	Metallation state of cSOD1	IEF, n= 9 PC, n=9 SEC+CF+IEF, n=9 SEC+IEF, n= 11	IEF, p= 0.06 Polycarbonate, p=0.519 SEC+CF+IEF, p=0.244 SEC+IEF, p=0.401	p=0.00034	Kruskall-Wallis p=4e-04 Multiple comparison with Dunn's test (IEF vs SEC+CF+IEF, p.adj= 0.00063) (PC vs SEC+CF+IEF, p.adj= 0.0097)

					(SEC+IEF vs SEC+CF+IEF, p.adj= 0.0034)
Supporting Figure S15	Cu/Zn atomic ratio of SOD1 from individual cases	-SEC individual cases: Case 1, n = 3 Case 2, n = 3 Case 3, n = 3 Case 4, n = 3 Case 5, n = 3 Case 6, n = 3 Case 7, n = 3 Case 8, n = 3			Kruskall-Wallis p=0.188
Supporting Figure S15	Cu/Zn atomic ratio of SOD1 from individual cases	-SEC individual cases: Case 9, n = 2 Case 10, n = 2 Case 11, n = 2 Case 12, n = 2 Case 13, n = 2 Case 14, n = 2 Case 15, n = 2 Case 16, n = 2 Case 17, n = 2			Kruskall-Wallis p=0.103

Supporting Table S13. Statistical analysis of data

Supporting Table S14. Mean Cu/Zn ratio of commercial cSOD1 (control) and active SOD1 dimers isolated from human occipital cortex (brain samples)

		Cu/Zn ratio		
	Procedure	Mean	Standard deviation (SD)	n
cSOD1	PC	0.93	0.01	9
Brain samples	IEF	2.39	1.42	23
Brain samples	SEC + IEF	1.12	0.28	18

Supporting Table S14. Mean Cu/Zn ratio of commercial cSOD1 (control) and active SOD1 dimers isolated from human occipital cortex (brain samples). Metal measurements were performed within the SOD1-containing gel band of focused IPG strips following native IEF. Measurement of SOD1 isolated from human brain tissue protein extracts using SXRF was performed on IPG strips loaded with SEC-processed and unprocessed brain tissue extracts. cSOD1 deposited onto polycarbonate foil (PC) was used as a positive control. Corresponding data depicted in Figure 2.

Supporting Figure S15. Boxplots median quartile and interquartile range for Cu/Zn atomic ratio of SOD1 from individual cases

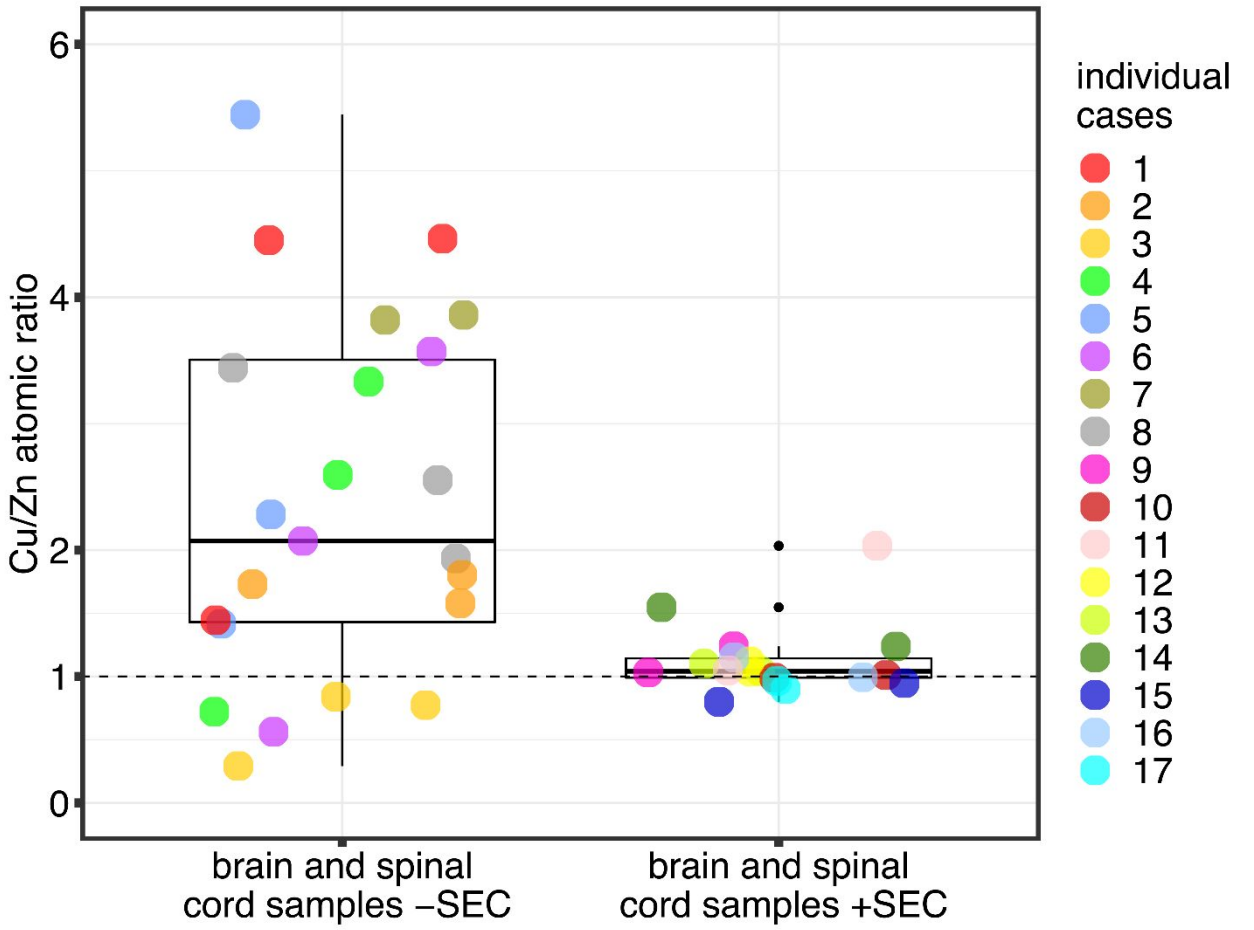

Supporting Figure S15. Boxplots median quartile and interquartile range for Cu/Zn atomic ratio from individual cases using native IEF alone (-SEC) and native 2D fractionation (+SEC). Data are from figure 2c and are color-coded according individual cases (17 cases). There were no statistically significant differences in Cu/Zn ratio between individual in the –SEC group. Similar result was found in the +SEC group. See Supporting Table S13 for details.

Supporting References S16

References cited in Supporting Information file.

(1) Trist, B. G.; Davies, K. M.; Cottam, V.; Genoud, S.; Ortega, R.; Roudeau, S.; Carmona, A.; De Silva, K.; Wasinger, V.; Lewis, S. J. G.; Sachdev, P.; Smith, B.; Troakes, C.; Vance, C.; Shaw, C.; Al-Sarraj, S.; Ball, H. J.; Halliday, G. M.; Hare, D. J.; Double, K. L. Amyotrophic Lateral Sclerosis-like Superoxide Dismutase 1 Proteinopathy Is Associated with Neuronal Loss in Parkinson's Disease Brain. *Acta Neuropathol.* **2017**, *134* (1), 113–127. https://doi.org/10.1007/s00401-017-1726-6.

(2) Davies, K. M.; Bohic, S.; Carmona, A.; Ortega, R.; Cottam, V.; Hare, D. J.; Finberg, J. P. M.; Reyes, S.; Halliday, G. M.; Mercer, J. F. B.; Double, K. L. Copper Pathology in Vulnerable Brain Regions in Parkinson's Disease. *Neurobiol. Aging* **2014**, *35* (4), 858–866. https://doi.org/10.1016/j.neurobiolaging.2013.09.034.

(3) Biagioli, M.; Pinto, M.; Cesselli, D.; Zaninello, M.; Lazarevic, D.; Roncaglia, P.; Simone, R.; Vlachouli, C.; Plessy, C.; Bertin, N.; Beltrami, A.; Kobayashi, K.; Gallo, V.; Santoro, C.; Ferrer, I.; Rivella, S.; Beltrami, C. A.; Carninci, P.; Raviola, E.; Gustincich, S. Unexpected Expression of α- and β-Globin in Mesencephalic Dopaminergic Neurons and Glial Cells. *Proc. Natl. Acad. Sci. U. S. A.* **2009**, *106* (36), 15454–15459. https://doi.org/10.1073/pnas.0813216106.

(4) Roudeau, S.; Chevreux, S.; Carmona, A.; Ortega, R. Reduced Net Charge and Heterogeneity of PI Isoforms in Familial Amyotrophic Lateral Sclerosis Mutants of Copper/Zinc Superoxide Dismutase. *Electrophoresis* **2015**, *36* (19). https://doi.org/10.1002/elps.201500187.

(5) Solé, V. A.; Papillon, E.; Cotte, M.; Walter, P.; Susini, J. A Multiplatform Code for the Analysis of Energy-Dispersive X-Ray Fluorescence Spectra. *Spectrochim. Acta Part B At. Spectrosc.* **2007**, *62* (1), 63–68. https://doi.org/10.1016/j.sab.2006.12.002.

(6) Campbell, J. L.; Boyd, N. I.; Grassi, N.; Bonnick, P.; Maxwell, J. A. The Guelph PIXE Software Package IV. *Nucl. Instruments Methods Phys. Res. Sect. B Beam Interact. with Mater. Atoms* **2010**, *268* (20), 3356–3363. https://doi.org/10.1016/j.nimb.2010.07.012.

(7) Carmona, a.; Devès, G.; Ortega, R. Quantitative Micro-Analysis of Metal Ions in Subcellular Compartments of Cultured Dopaminergic Cells by Combination of Three Ion Beam Techniques. *Anal. Bioanal. Chem.* **2008**, *390* (6), 1585–1594. https://doi.org/10.1007/s00216-008-1866-6.

(8) Käll, L.; Canterbury, J. D.; Weston, J.; Noble, W. S.; MacCoss, M. J. Semi-Supervised Learning for Peptide Identification from Shotgun Proteomics Datasets. *Nat. Methods* **2007**, *4* (11), 923–925. https://doi.org/10.1038/nmeth1113.

(9) RStudio Team. RStudio: Integrated Development Environment for R. Boston, MA 2020.

(10) R Core Team. R Foundation for Statistical Computing. R: A Language and Environment for Statistical Computing. Vienna, Austria 2019.

(11) Wickham, H.; Averick, M.; Bryan, J.; Chang, W.; McGowan, L.; François, R.; Grolemund, G.; Hayes, A.; Henry, L.; Hester, J.; Kuhn, M.; Pedersen, T.; Miller, E.; Bache, S.; Müller, K.; Ooms, J.; Robinson, D.; Seidel, D.; Spinu, V.; Takahashi, K.; Vaughan, D.; Wilke, C.; Woo, K.; Yutani, H. Welcome to the

Tidyverse. *J. Open Source Softw.* **2019**, *4* (43), 1686. https://doi.org/10.21105/joss.01686.

(12) Fox, J.; Bouchet-Valat, M. Rcmdr: R Commander. 2020.

(13) Pergande, M.; Cologna, S. Isoelectric Point Separations of Peptides and Proteins. *Proteomes* **2017**, *5* (4), 4. https://doi.org/10.3390/proteomes5010004.

(14) Lago, L.; Thomas, O. R. B.; Roberts, B. R. Choice of Mobile Phase: Implications for Size Exclusion Chromatography-Inductively Coupled Plasma-Mass Spectrometry Analyses of Copper, Zinc and Iron Metalloproteins. *J. Chromatogr. A* **2020**, *1616*, 460806. https://doi.org/10.1016/j.chroma.2019.460806.